

Special Collection: 40 Years of Colloidal Nanocrystals in JCP

Conan Huang 📵 ; Yiran Jiang 📵 ; Gryphon A. Drake 💿 ; Logan P. Keating 💿 ; Moonsub Shim 🗷 📵



J. Chem. Phys. 158, 244701 (2023) https://doi.org/10.1063/5.0147782





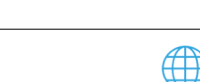
CrossMark





Improving photovoltaic performance of light-responsive double-heterojunction nanorod light-emitting diodes 💷 🕫

Cite as: J. Chem. Phys. 158, 244701 (2023); doi: 10.1063/5.0147782 Submitted: 26 February 2023 • Accepted: 10 April 2023 •





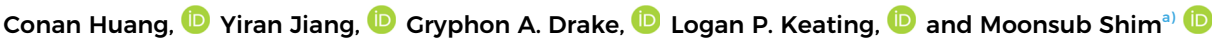




Published Online: 22 June 2023









AFFILIATIONS

Department of Materials Science and Engineering, University of Illinois at Urbana-Champaign, Urbana, Illinois 61801, USA

Note: This paper is part of the JCP Special Topic on 40 Years of Colloidal Nanocrystals in JCP.

a) Author to whom correspondence should be addressed: mshim@illinois.edu

ABSTRACT

Double heterojunction nanorods enable both electroluminescence and light harvesting capabilities within the same device structure, providing a promising platform for energy-scavenging displays and related applications. However, the efficiency of the photovoltaic mode remains modest for useful power conversion and may be challenging to improve without sacrificing performance in electroluminescence. Through a facile on-film partial ligand exchange with benzenethiol integrated into the device fabrication step, we achieve an average of more than threefold increase in power conversion efficiency while maintaining the maximum external quantum efficiency and the maximum luminance in the LED mode. The improved photovoltaic performance is mainly due to the increase in the short circuit current, which we attribute to the enhanced charge separation afforded by the partial ligand exchange. The recovery of the photoluminescence lifetime under the forward bias suggests that the hole traps introduced by benzenethiols are filled prior to reaching the voltage at which light emission begins, allowing LED performance to be maintained and possibly improved.

Published under an exclusive license by AIP Publishing. https://doi.org/10.1063/5.0147782

I. INTRODUCTION

Emerging anisotropic heterostructures of semiconductor nanocrystals or colloidal quantum dots (QDs) provide exciting opportunities to manipulate charge carrier flow, separation, and recombination with nanoscale precision, paving the path to novel electronic, optoelectronic, and photovoltaic devices. One such structure, the double heterojunction nanorod (DHNR), exemplifies simultaneous advantages that arise from a combination of nanoscale band structure engineering and shape anisotropy.^{8–12} When used as electroluminescent materials in light-emitting diodes (LEDs), the band offsets designed into DHNRs improve charge injection, while their rod shape enhances light outcoupling.9 Furthermore, DHNRs impart a new capability of being able to operate as photodetectors—i.e., individual LED pixels that can operate in both light emitting and detecting modes directly without added components.¹¹ The photocurrent is generated by the photovoltaic (PV) effect, and the band structure designed into them may be exploited to improve PV performance without sacrificing LED

characteristics. In addition, these devices may be patterned into large emissive pixel arrays by simple solution processing or transfer printing. 13-15 These salient features of DHNRs can lead to a broad range of applications. For example, light harvesting capability can be implemented directly using emissive pixels of display screens without the need for separate solar cells.

While the PV response of DHNR-LEDs provides sufficient photocurrent for light sensing, 11 a significant improvement is needed for useful power conversion. However, improving the PV response while maintaining high LED performance is largely unexplored and can be very challenging. Typical QD-LEDs utilize type-I straddling band offset core/shell structures to confine charges to enhance radiative recombination. 16-19 In contrast, QD-based solar cells often require closely packed core nanocrystals without an inorganic shell to enhance charge extraction and transport.²⁰ Hence, improving one process can be detrimental to the other. Photogenerated charges in DHNRs may be more easily separated due to quasi-type II band offsets, and their lifetimes can be quite long,²¹ yet DHNR-LEDs exhibit excellent light emitting characteristics.

Hence, DHNRs may not be limited in the same way as core/shell QDs, and these features provide a potential opportunity to simultaneously improve both PV and EL characteristics.

In order to achieve efficient charge injection and transport for the LED mode, the thickness of the DHNR film in the device needs to be one to a few layers of nanorods. Given this limitation, one approach to improving PV response is through surface modification of DHNRs. The "native" capping molecules on the surface of DHNRs (and more generally, for most colloidal nanoparticles²²) are optimized for synthesis, during which the ligands help to control the reactivity of precursors and the surface of growing crystals. However, typical native ligands, such as trioctylphosphine (TOP), trioctylphosphine oxide (TOPO), octadecylphosphonic acid (ODPA), and oleic acid (OA), have long alkyl chains that do not permit for efficient injection, extraction, and transport of charge carriers. Ligand exchange can improve electrical conductivity, ^{23–30} facilitate charge injection/extraction through surface dipole induced modulation of energy level position, 31,32 and facilitate charge separation. 33-36 Combining the benefits of enhanced charge transport and more favorable energy band alignment, ligand exchange has been especially successful for improving the performance of QD solar cells.²⁰ Large depletion regions,³⁷ efficient charge extraction,³⁸ and air stability^{36,39} have been achieved through different ligand exchange processes. Enhanced charge separation and stability have also been imparted through ligand exchange in colloidal nanorod heterostructure based solar cells.35

The effects of ligand exchange on the EL characteristics of QDs and related materials have been much less explored and can be more complex due to multiple effects that ligands can impart. In particular, ligand exchange can often lead to reduced PL, which is usually strongly related to EL. For example, shorter chain molecules can improve charge transport in QD-LEDs, 40-42 but the resulting reduced interparticle spacing can lead to Forster energy transfer that can reduce PL and, in turn, EL. 43,44 Surface electric dipoles induced by ligand exchange with thiols have been suggested to reduce the hole injection barrier and improve the performance of QD-LEDs. 45-49 However, thiols are considered to be hole-trapping ligands for CdSe QDs, which means they can quench PL. 50 Exchanging the native Cd-carboxylate ligands with alkyl amines has been shown to improve LED performance and device lifetime through the elimination of surface Cd²⁺ to Cd⁰ reduction upon electron injection that quenches PL.51 On the other hand, certain amine ligands, including commonly used oleylamine, have been shown to lead to transient overshoot in EL, which has been attributed to charge storage/trapping at the QD-ligand interface.⁵² Hence, to enhance the PV response of DHNR-LEDs while also improving LED performance, the enhancements in charge separation, injection, extraction, and/or transport that may be afforded by ligand exchange must be considered along with potential surface charge trapping that can lead to degradation of PL and EL.

Here, we examine the effects of partial ligand exchange using benzenethiol (BT) on the PV and EL characteristics of DHNR-LEDs. The improvement in power conversion efficiency (PCE) arises mainly from increased short circuit current. Voltage-dependent current density and PL lifetime measurements suggest that the main contribution to the increase in the short circuit current is likely due to the enhancement of charge separation arising from a limited

number of hole traps introduced by BT. As indicated by the recovery of PL lifetime, these trap states are filled with the forward bias below the LED turn-on voltage, simultaneously allowing LED performance to be maintained or possibly even improved despite the introduction of hole traps.

II. METHODS

A. Materials

Trioctylphosphine oxide (TOPO) (99%), trioctylphosphine (TOP) (90%), oleic acid (OA) (90%), octadecene (ODE) (90%), CdO (99.5%), Zn acetate (99.99%), S powder (99.998%), Se powder (99.99%), benzenethiol (\geq 99%), ethanol (anhydrous, \geq 99.5%) octane (anhydrous, \geq 99.9%), and m-xylene (anhydrous, 99%) were purchased from Sigma-Aldrich. N-octadecylphosphonic acid (ODPA) was purchased from PCI synthesis. ACS grade chloroform and methanol were purchased from Fischer Scientific. Poly[(9,9-dioctylfluorenyl-2,7-diyl)-co-(4,4'-(N-(4-sec-butylphenyl)diphenylamine))] (TFB) packed under Ar was purchased from H.W. Sands Corp. ITO substrates and poly(3,4-ethylenedioxythiophene)-poly(styrenesulfonate) in water (PEDOT:PSS, AI8043) were purchased from Ossila.

B. Synthesis of CdS/CdSe/ZnSe double-heterojunction nanorods (DHNRs)

The barbell-shaped CdS/CdSe nanorods were synthesized following Ref. 21. Briefly, 2 mmol CdO, 4 mmol ODPA, and 8 g TOPO (99%) were added to a 100 ml round-bottom flask and degassed at 150 $^{\circ}$ C for 30 min. The reaction mixture was then heated to 380 $^{\circ}$ C under Ar flow until the solution became clear, at which point 1 mmol of S dissolved in 6 ml of TOP (99%) was injected swiftly into the flask and allowed to stir for 15 min. The reaction mixture was then cooled to 250 $^{\circ}$ C, and 0.5 mmol of Se dissolved in 2 ml of TOP was added dropwise into the flask at 7.5 ml/h and allowed to stir for 10 min. The reaction mixture was then cooled to room temperature and purified by centrifugation using ethanol and hexanes and redispersed into hexanes for the next step.

The purified reaction mixture dispersed in hexanes was added to a solution of 4 mmol of $Zn(ac)_2$, 16 mmol of oleic acid (OA), and 20 ml of 1-ODE. Hexanes was evaporated, and the reaction mixture was then degassed for 1 h under vacuum at $100\,^{\circ}$ C. The temperature was then raised to 250 $^{\circ}$ C under Ar. As the reaction mixture was heating up, at $180\,^{\circ}$ C, 0.15 mmol Se dissolved in 1.5 ml of TOP was added dropwise at 6 ml/h. Subsequently, the reaction mixture was allowed to heat up to and stir at 250 $^{\circ}$ C for 30 min and then cooled to room temperature. The resulting reaction mixture was purified via centrifugation using ethanol and hexanes. The resulting pellet of CdS/CdSe nanorod heterostructures was dried and redispersed in TOP in an N_2 filled glove box.

To grow the ZnSe shell, a solution of CdS/CdSe nanorod heterostructures (NRHs) and Se in TOP was prepared. The ratio of NRH to Se was maintained in the following way. The dried NRHs were first dissolved in 18 ml hexanes, and the optical density at the CdSe first exciton transition was measured (typically, ~0.045 in a 1-cm path length cuvette when diluted 30-fold). The NRHs were then precipitated using ethanol, dried, and dissolved in a 0.6M solution of Se in TOP. The volume of TOP-Se solution is adjusted to maintain the ratio of optical density to the number of moles of Se to

0.05. In a separate flask, a solution of 3 mmol of Zn(ac)₂, 12 mmol of OA, and 15 ml of 1-ODE was degassed at 100 °C for 1 h and subsequently heated to 300 °C under Ar. The solution of CdS/CdSe NRHs and Se in TOP was then swiftly injected into the flask, and the reaction mixture was allowed to stir for 5 min at 300 °C and then cooled to room temperature. The resulting CdS/CdSe/ZnSe DHNRs were purified by precipitation using a solvent mixture of CHCl₃ and acetonitrile followed by centrifugation. The supernatant was discarded, and the precipitate was re-dispersed in octane for device fabrication (typically, 0.4 ml of octane per 1 ml of reaction mixture).

C. Device fabrication

After cleaning with acetone and isopropanol, and treatment under a UV-ozone lamp for 15 min, pre-patterned ITO/glass substrates were used for fabricating LEDs. PEDOT:PSS was spin-cast directly onto the ITO at 4000 rpm for 30 s and then baked at 135 °C for 5 min in air. All subsequent steps were carried out in an N₂ filled glovebox. TFB (H.W. Sands Corp.) dissolved in m-xylene (8 mg/ml) was spin-cast at 3000 rpm for 30 s and then baked at 150 °C on a hotplate for 30 min. The DHNR solution was then spincast at 2000 rpm for 30 s. On-film ligand exchange was performed by flooding the surface with BT dissolved in ethanol for 15 s before spin-cast drying at 2000 rpm. The optimum BT concentration varied from device batch to batch but lied between 0.1% and 1% v/v for all cases examined here. Ethanol was then spin-cast twice to remove the excess ligands. The DHNR films were annealed at 180 °C for 30 min after the partial ligand exchange step. Subsequently, colloidal ZnO solution (~30 mg/ml in butanol, prepared following reported method⁵³) was spin-cast at 2000 rpm for 30 s and baked at 110 °C for 30 min. Finally, 100 nm thick Al cathodes were defined by a shadow mask and deposited by thermal evaporation. LEDs were encapsulated with a glass cover slip using an epoxy (NOA 86) in the glovebox.

D. Characterization

The thicknesses of the DHNR films were estimated with a J. A. Woollam VASE ellipsometer. DHNR films were prepared on Si substrates using the same conditions as device fabrication, and ellipsometry data were collected in the wavelength range of 400-900 nm at an incidence angle of 60°. Data analysis was performed using WVASE32 software. The thickness of the films was determined to be ~45 nm using the Cauchy model. All LED characteristics were recorded using a Spectrascan PR-655 spectroradiometer coupled with a Keithley 2602B source-measure unit. External quantum efficiency (EQE) was calculated as the ratio of the number of photons emitted (calculated from luminance measured by the spectroradiometer) to the numbers of electrons injected (calculated from measured current). Current and power efficiencies were obtained as the ratio of the output luminance to the driving current density and the ratio of the luminous flux output to the driving electrical power, respectively. Photovoltaic characteristics were recorded under the AM 1.5 (100 mW/cm²) condition using a Newport solar simulator. Time-resolved PL was measured using a Horiba Nanolog spectrofluorometer with 400 nm pulsed diode laser. Weighted average PL lifetimes⁵⁴ were calculated from three-exponential fits to the data. All device measurements were performed in air.

III. RESULTS AND DISCUSSION

While there are compelling reasons that ligand exchange can improve the photovoltaic response of DHNRs based on previous reports on QD solar cells, ^{20,24,25,32,55} simultaneously maintaining or improving LED performance appears to be a much more difficult challenge. Many ligands, including thiols, can act as charge traps, which can reduce PL and, in turn, EL. In addition, the ligand exchange process, when carried out in solution, usually requires several purification cycles, which can easily degrade PL. Nevertheless, partial ligand exchange with thiols, including benzenethiol (BT), has been shown to lead to improvement in EL characteristics of QD-LEDs. ^{45,46} However, it remains unclear if and how ligand exchange with thiols might lead to improvement in both PV and LED performance of light-responsive DHNR-LEDs.

As-synthesized DHNRs examined here consist of CdS nanorods with CdSe tips passivated with ZnSe and are capped mainly with oleic acid (see Sec. II for details). The double heterostructure band alignment of these components within the DHNR facilitate both carrier injection and extraction, while the anisotropic rod shape can enhance light outcoupling.¹⁰ Figure 1 shows the expected band diagram and LED characteristics of a control DHNR-LED fabricated without any BT treatment. A schematic of the device structure and a TEM image of DHNRs are shown in the lower-left and lower-right insets of Fig. 1(a), respectively. PL in solution and EL during device operation at different voltages are shown in Fig. 1(b). Current density (J) and luminance (L) vs voltage (V) characteristics are shown in Fig. 1(c). The corresponding external quantum efficiency (EQE) for the LED mode is plotted in Fig. 1(d). As the band diagram illustrates, the CdS rod with commensurate conduction band alignment with the ZnO electron transport layer facilitates electron injection and the ZnSe shell reduces the barrier for hole injection from the TFB hole transport layer. This advantage of the double heterostructure band alignment of DHNRs has also been attributed to imparting photocurrent generation capability in DHNR-LEDs.1

We first compare control (native ligands) and BT-treated devices fabricated in parallel from the same batch of DHNRs using the same reagent solutions in order to minimize complications from potential device-to-device variations. The only difference in the device fabrication process is an on-film partial ligand exchange step with BT (see Sec. II). Figure 2 shows the characteristics of two such devices. Treatment with the shorter BT ligands does not cause any significant changes in the peak position or the width in the EL spectrum, as shown in Fig. 2(a). It does lead to an overall higher current density [Fig. 2(b)]. As the logarithmic plot of current density in the inset shows, the BT-treated device exhibits slightly lower shunt resistance as evidenced by the higher current in the ohmic regime. However, the slope of the J-V curve from just below 2–3 V remains the same, indicative of insignificant effect from the partial ligand exchange with respect to trap-limited transport when the LED reaches the light emitting voltage range. The overall increase in the current density is accompanied by higher luminance [Fig. 2(c)]. The maximum luminance is slightly higher by 7.5% (66 300 cd/m² compared to 61 700 cd/m²) for the BT-treated device. Hence, this on-film partial ligand exchange appears to have little effect on the LED performance.

Despite the small difference in EL characteristics, BT-treatment leads to a significant increase in the photocurrent [Fig. 2(d)]. The

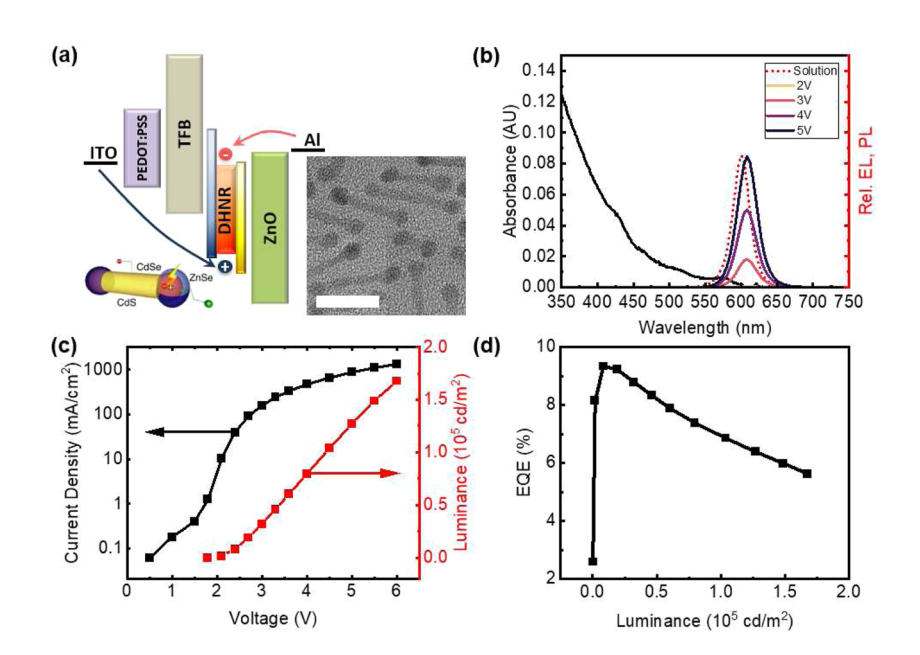


FIG. 1. (a) Expected band diagram for the control light-responsive DHNR-LED along with a schematic and TEM image (scale bar is 20 nm) of the DHNRs with native ligands. (b) Solution PL (dotted line) and absorption spectra (black solid line) along with normalized EL spectra (colored solid lines) acquired with a driving voltage from 2 to 5 V as indicated. (c) Log-linear scale plot of current density (black) and linear scale luminance (red) vs bias voltage. (d) Dependence of external quantum efficiency (EQE) of the DHNR device on luminance.

BT-treated device exhibits short circuit current (0.52 mA/cm²) that is nearly three times as large as that of the control device (0.19 mA/cm²). Analysis of dark current J-V characteristics as shown in Fig. S1 (see the supplementary material for curve fitting details) indicates that series resistance is similar for these two devices (1.4 Ω /cm² for BT-treated vs 1.5 Ω /cm² for control). The open circuit voltage (1.47 vs 1.35 V) and the fill factor (27.0 vs 27.3%) are also similar. The net effect is that the PCE is about three times higher for the BT-treated device, mainly due to the larger short circuit current.

While the improvement in the PV response without sacrificing LED performance with the simple on-film thiol treatment in these particular DHNR-LEDs is highly promising, device-to-device variations must be taken into consideration before conclusions can be made. To this end, we have examined DHNR-LEDs with and without BT treatment that exhibit a range of PV and LED performances. Figures 3(a) and 3(b) compare the PCE of DHNRs with and without BT-treatment for two different device metrics: maximum EQE in the LED mode and short circuit current in the PV mode.

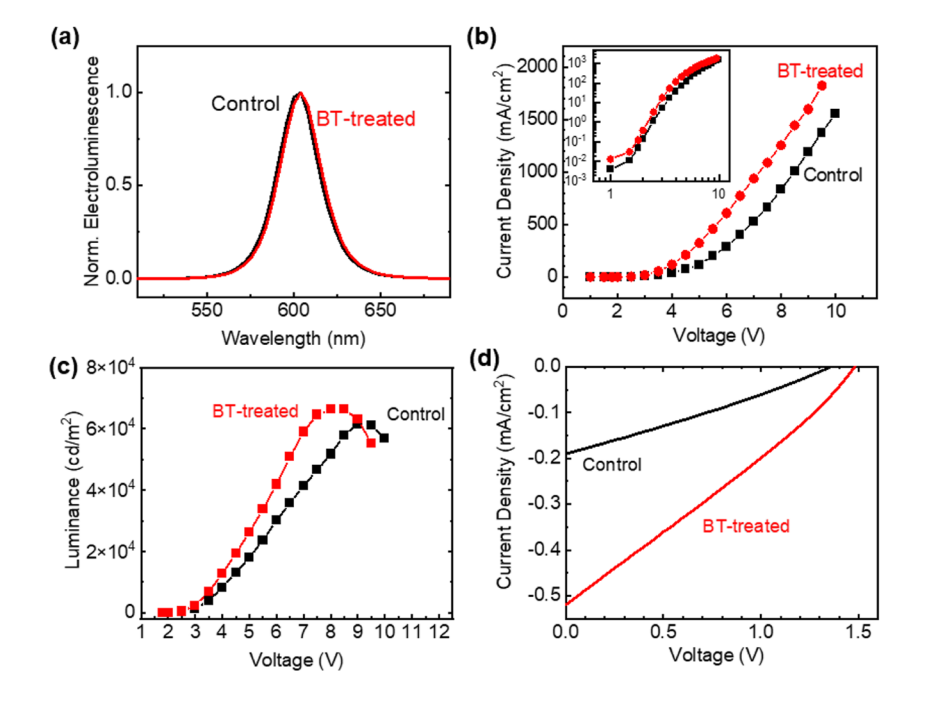


FIG. 2. (a) Electroluminescence spectra of control (black) and BT-treated (red) devices operating at 3 V. (b) Plot of the current density vs voltage characteristics (J–V) of control (black) and BT-treated (red) devices. The log–log scale plot of the same data is shown in the inset. (c) Luminance vs voltage characteristics (L–V) of control (black) and BT-treated (red) devices. (d) Photocurrent as a function of voltage for control (black) and BT-treated (red) DHNR devices measured under AM1.5 G (100 mW/cm²) conditions.

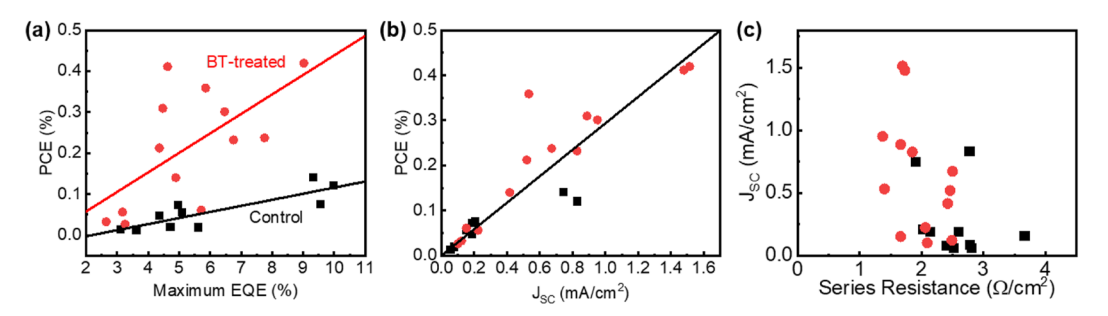


FIG. 3. (a) Device statistics comparing correlation of PCE with the maximum EQE of the LED mode for light-responsive DHNR-LEDs with and without BT treatment. Linear fits show a steeper slope (0.048 vs 0.015) and, therefore, stronger dependence of PCE on the LED-mode EQE for the BT-treated devices. (b) Dependence of PCE on the short circuit current (J_{SC}). (c) The distribution of J_{SC} with respect to series resistance. In all cases, red circles and black squares correspond to devices with and without BT-treatment, respectively.

Figure 3(a) shows that there is a positive correlation of PCE under the PV mode of operation with the maximum EQE in the LED mode. While both the control and BT-treated devices span a similar range of maximum EQE values, the PCE of the BT-treated devices exhibits stronger dependence. The lowest EQE cases show low PCE regardless of ligand treatment. However, as the maximum EQE in the LED mode becomes higher, the dependence of PCE differentiates substantially. The solid lines are linear fits to the data for each type, and the BT-treated devices show ~4 times steeper slope. These results are especially encouraging in that fabricating better LEDs can lead to greater improvement in PV performance.

As with the individual device comparisons in Fig. 2, the main factor that improves the PCE is the larger short circuit current. Figure 3(b) shows that the PCE is strongly correlated with the short circuit current and BT-treated devices tend to exhibit larger short circuit current. The open circuit voltage does not appear to be affected significantly by the partial ligand exchange step as both the control and the BT-treated devices span a similar range of open circuit voltages, and there is no obvious correlation to PCE (Fig. S2a). The average (~25%) and the range (10%-50%) of fill factor values also remain similar regardless of BT treatment (Fig. S2b). As is the case for the individual device comparison in the inset of Fig. 2(b), the distribution of the slope of the trap-limited regime of the logarithmic J-V plot remains similar as well (Fig. S2c). Series resistance measured from the dark current also does not appear to be significantly affected by the ligand treatment, as shown in Fig. 3(c). BT-treated devices have a slightly lower average series resistance of 2.0 Ω/cm^2 compared to control devices with an average of 2.6 Ω/cm^2 . Since the composition and the thicknesses of the metal contacts and the charge transport layers are the same, the lower average series resistance may indicate reduced contact resistance between the DHNR film and the charge transport layers. However, the small difference cannot account for more than a factor of 2 larger average short circuit current seen upon BT treatment (0.65 vs 0.28 mA/cm²).

Given that photon absorption should be nominally the same due to similar thickness and optical density, the increase in the short circuit current, which is the main reason for the higher PCE, is likely arising from improvements in charge transport and/or charge separation within the DHNR layer. However, the above results suggest that BT treatment leads to a minor improvement in charge transport.

Then, to better understand how PCE can be improved with a minimal effect on LED performance, time-resolved PL measurements under applied bias were carried out. The PL intensity decay over time of the control and thiol-treated devices under different applied voltages are shown in Figs. 4(a) and 4(b), respectively. The limit of the forward bias is set to be below the LED turn-on such that EL does not contribute to the signal. The dependence of the weighted average PL lifetime on the applied voltage is shown in Fig. 4(d). In both cases, slower PL decay is observed as the applied voltage is increased toward the voltage at which the LED turns on. It is the decrease in the amplitude of the fastest component that leads to longer PL lifetime.

For the control device, the increase in the PL lifetime with the increasing forward bias has been attributed to the applied voltage counteracting the band alignment that allows for efficient separation of photogenerated charges. ¹¹ The PL lifetime measured when the device circuit is left electrically floating (black filled star labeled "open circuit") is approximately the same as when the applied voltage is set to the open circuit voltage at ~1.5 V rather than being similar to when the device is shorted at 0 V. This phenomenon has been explained by photogenerated carriers remaining in the DHNR layer when the circuit is floating or set to the open circuit voltage, leading to longer PL lifetime, whereas they are separated and transported away as photocurrent, leading to shorter PL lifetime when the circuit is at voltages below the open circuit voltage. ¹¹

The BT-treated device shows similar dependence on the applied bias (i.e., increasing PL lifetime with the increasing forward bias), but there are distinct differences. With the introduction of hole-trapping thiols on the surface of DHNRs, faster PL decay is expected and is evident in the shorter PL lifetime observed for most of the voltage range examined and when the device is electrically floating. In addition, the PL lifetime when the device is electrically floating, while slightly longer than when the device is shorted at 0 V, no longer corresponds to the PL lifetime at the open circuit voltage. This result may be expected if the hole traps introduced by BT ligands lead to additional non-radiative recombination pathways that are present even if the photogenerated charges are not carried away as photocurrent. The substantial increase in the photocurrent despite the introduction of hole-trapping thiol molecules on the surface of DHNRs may be explained by the hole trap levels

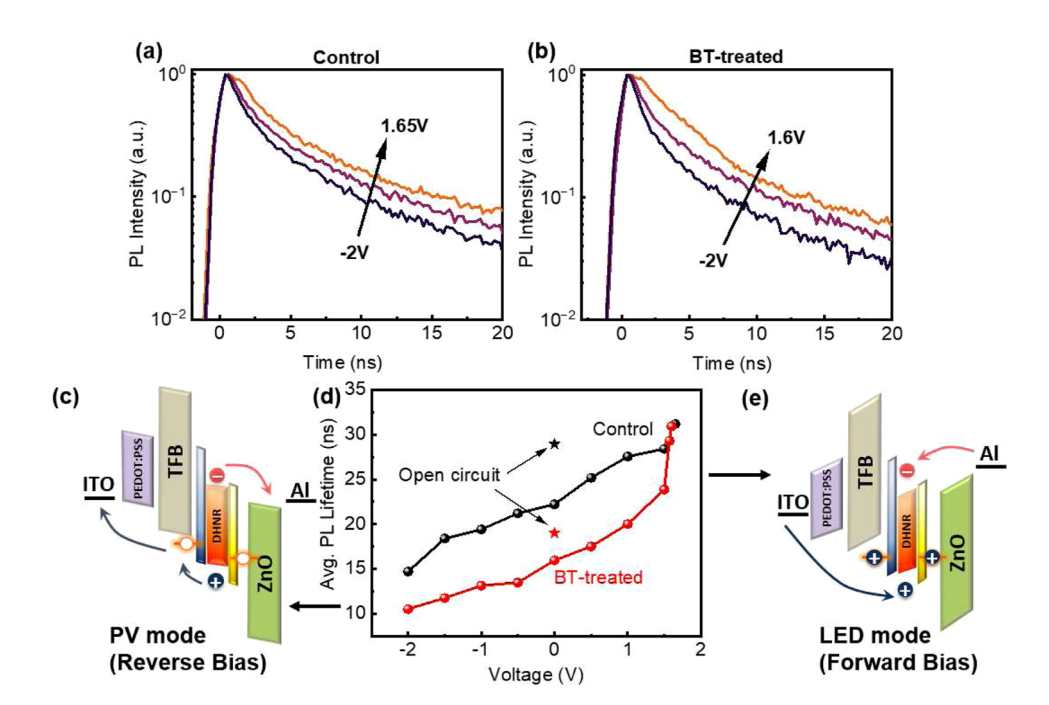


FIG. 4. Time-resolved PL measurements on control (a) and BT-treated (b) devices under the indicated bias. (d) Bias-dependent weighted average PL lifetime of control (black symbols) and BT-treated (red symbols) DHNR devices. Star symbols correspond to PL lifetime when the devices are electrically floating ("open circuit"). (c) and (e) Schematics showing the band alignment under the applied bias for a BT-treated device illustrating the potential effect of hole traps introduced by BT ligands for the PV mode (left schematic) and for the LED mode (right schematic). The recovery of PL lifetime in BT-treated devices to the same value as the control case at ~1.5 V, which is just below the voltage at which light-emission initiates, suggests that hole traps introduced by BT are filled, allowing for LED operation without performance degradation due to these hole traps.

being positioned in between the valence band edges of CdSe/ZnSe of DHNRs and the hole transport layer, TFB. Hence, the surface trapped hole is still energetically favorable to transfer into TFB [PV mode band diagram of Fig. 4(c)], effectively allowing BT ligands to enhance the separation of photogenerated charges.

While the above observations can explain how the partial ligand exchange with BT can improve the PV response of DHNR-LEDs, it is unclear how introducing hole traps can enhance or at least maintain performance in the LED mode. The bias dependence comparison in Fig. 4(d) shows that the PL lifetime of the BT-treated device increases to the same value as that of the control device near the open circuit voltage or just below the LED turn-on. Other BT-treated devices that show enhanced PCE exhibit this recovery in PL lifetime, but because of device-to-device variations, the degree of recovery can vary. Another example of bias-dependent PL lifetime of control vs BT-treated device comparison is shown in Fig. S3. One possible explanation for PL lifetime recovery under the forward bias is that the hole traps are progressively filled with the increasing forward bias such that when the LED begins to emit [Fig. 4(e)], the radiative recombination efficiency of BT-treated DHNRs becomes similar to that of the untreated control case. The hole traps introduced by thiols may even provide a gradient of hole states that may facilitate the hole injection process. However, the number of hole traps introduced must be limited such that they can be filled prior to the LED turn-on voltage being reached. This effect may be the reason why we observe declining performance when high BT concentration solution is used for the on-film ligand exchange step. These results suggest a potential path to further improve PV and EL efficiencies of DHNR-LEDs simultaneously through a simple partial ligand exchange approach.

Finally, we note that preliminary studies on incident-photonto-current efficiency (IPCE) indicate that the improvement in the photovoltaic response occurs over the entire spectral range where DHNRs and the charge transport layers absorb light (Fig. S4). The increase in IPCE arising from photoexcitation of ZnO ETL can be expected if BT enhances charge separation across the ZnO/DHNR interface via the introduced hole traps similar to photoexcitation in DHNRs. However, it is unclear at this stage how BT-treatment might affect charge separation across the TFB/DHNR interface and further studies, including statistics on device-to-device variations, are warranted to elucidate such effects.

IV. CONCLUSIONS

In summary, we have shown that a simple on-film partial ligand exchange with the short aromatic thiol molecule, BT, can lead to a significant improvement in the PCE of light-responsive DHNR-LEDs. The PCE is correlated with the maximum EQE of the LED mode, indicating that fabricating better LEDs will lead to better PV responses. On average, more than a threefold increase in PCE has been observed without sacrificing LED performance. The partial ligand exchange reduces both the series and shunt resistances slightly, but the majority of the enhancement arises from the increase in the short circuit current. The main impact of the BT-treatment appears to be in enhancing charge separation as suggested by the bias-dependent PL lifetime comparison. The recovery of PL lifetime upon forward driving voltage indicates that the limited number of hole traps, introduced by partial ligand exchange with BT, may be filled prior to reaching the LED turn-on voltage. Hence, the PV response can be improved, while the LED efficiency is maintained. These hole traps may even be exploited in the future to facilitate hole injection and extraction to improve both PV and LED performances simultaneously.

SUPPLEMENTARY MATERIAL

See the supplementary material for details of curve fitting to determine series resistance, device statistics on open circuit voltage, fill factor, and trap-limited transport and an additional example of bias-dependent PL lifetime.

ACKNOWLEDGMENTS

Financial support from the U.S. National Science Foundation (Grant No. 2132538) is gratefully acknowledged. Experiments were carried out, in part, in the Frederick Seitz Materials Research Laboratory Central Facilities, University of Illinois.

AUTHOR DECLARATIONS

Conflict of Interest

The authors have no conflicts to disclose.

Author Contributions

Conan Huang and Yiran Jiang authors contributed equally.

Conan Huang: Conceptualization (equal); Data curation (equal); Formal analysis (equal); Investigation (equal); Writing – original draft (equal); Writing – review & editing (equal). Yiran Jiang: Conceptualization (equal); Data curation (equal); Formal analysis (equal); Investigation (equal); Writing – original draft (equal); Writing – review & editing (equal). Logan P. Keating: Formal analysis (supporting); Writing – review & editing (equal). Logan P. Keating: Formal analysis (supporting); Writing – review & editing (equal). Moonsub Shim: Conceptualization (lead); Formal analysis (equal); Funding acquisition (lead); Project administration (lead); Supervision (lead); Writing – original draft (lead); Writing – review & editing (lead).

DATA AVAILABILITY

The data that support the findings of this study are available from the corresponding author upon reasonable request.

REFERENCES

- ¹J. Y. Kim, O. Voznyy, D. Zhitomirsky, and E. H. Sargent, Adv. Mater. 25, 4986 (2013).
- ²D. V. Talapin, J.-S. Lee, M. V. Kovalenko, and E. V. Shevchenko, Chem. Rev. 110, 389 (2010).
- ³P. V. Kamat, J. Phys. Chem. C 112, 18737 (2008).
- ⁴C. J. Stolle, T. B. Harvey, and B. A. Korgel, Curr. Opin. Chem. Eng. 2, 160 (2013).
- ⁵M. J. Enright and B. M. Cossairt, Chem. Commun. **54**, 7109 (2018).
- ⁶G. A. Drake, L. P. Keating, and M. Shim, Chem. Rev. 123, 3761 (2023).
- ⁷Y. Jiang, S.-Y. Cho, and M. Shim, J. Mater. Chem. C 6, 2618 (2018).
- ⁸N. Oh, S. Nam, Y. Zhai, K. Deshpande, P. Trefonas, and M. Shim, Nat. Commun. 5, 3642 (2014).
- ⁹S. Nam, N. Oh, Y. Zhai, and M. Shim, ACS Nano 9, 878 (2015).
- $^{\bf 10}$ Y. Jiang, N. Oh, and M. Shim, ACS Photonics 3, 1862 (2016).

- ¹¹N. Oh, B. H. Kim, S.-Y. Cho, S. Nam, S. P. Rogers, Y. Jiang, J. C. Flanagan, Y. Zhai, J.-H. Kim, J. Lee, Y. Yu, Y. K. Cho, G. Hur, J. Zhang, P. Trefonas, J. A. Rogers, and M. Shim, Science 355, 616 (2017).
- ¹²S.-Y. Cho, N. Oh, S. Nam, Y. Jiang, and M. Shim, Nanoscale **9**, 6103 (2017).
- ¹³ B. H. Kim, S. Nam, N. Oh, S.-Y. Cho, K. J. Yu, C. H. Lee, J. Zhang, K. Deshpande, P. Trefonas, J.-H. Kim, J. Lee, J. H. Shin, Y. Yu, J. B. Lim, S. M. Won, Y. K. Cho, N. H. Kim, K. J. Seo, H. Lee, T.-i. Kim, M. Shim, and J. A. Rogers, ACS Nano 10, 4920 (2016).
- ¹⁴ H. Keum, Y. Jiang, J. K. Park, J. C. Flanagan, M. Shim, and S. Kim, ACS Nano 12, 10024 (2018).
- ¹⁵ M. K. Choi, J. Yang, K. Kang, D. C. Kim, C. Choi, C. Park, S. J. Kim, S. I. Chae, T.-H. Kim, J. H. Kim, T. Hyeon, and D.-H. Kim, Nat. Commun. 6, 7149 (2015).
- ¹⁶H. Jung, Y.-S. Park, N. Ahn et al., Nat. Commun. 13, 3734 (2022).
- ¹⁷Y. Shu, X. Lin, H. Qin, Z. Hu, Y. Jin, and X. Peng, Angew. Chem., Int. Ed. 59, 22312 (2020).
- ¹⁸D. Hahm, J. Lim, H. Kim et al., Nat. Nanotechnol. **17**, 952 (2022).
- ¹⁹T. Kim, K.-H. Kim, S. Kim, S.-M. Choi, H. Jang, H.-K. Seo, H. Lee, D.-Y. Chung, and E. Jang, Nature **586**, 385 (2020).
- ²⁰M. Yuan, M. Liu, and E. H. Sargent, Nat. Energy 1, 16016 (2016).
- ²¹ G. A. Drake, J. C. Flanagan, and M. Shim, J. Chem. Phys. **151**, 134706 (2019).
- ²²M. A. Boles, D. Ling, T. Hyeon, and D. V. Talapin, Nat. Mater. 15, 141 (2016).
- ²³D. Yu, C. Wang, and P. Guyot-Sionnest, Science **300**, 1277 (2003).
- ²⁴Y. Wang, J. Yuan, X. Zhang, X. Ling, B. W. Larson, Q. Zhao, Y. Yang, Y. Shi, J. M. Luther, and W. Ma, Adv. Mater. 32, 2000449 (2020).
- ²⁵ M. Biondi, M.-J. Choi, S. Lee, K. Bertens, M. Wei, A. R. Kirmani, G. Lee, H. T. Kung, L. J. Richter, S. Hoogland, Z.-H. Lu, F. P. García de Arquer, and E. H. Sargent, ACS Energy Lett. 6, 468 (2021).
- ²⁶ A. T. Fafarman, W.-K. Koh, B. T. Diroll, D. K. Kim, D.-K. Ko, S. J. Oh, X. Ye, V. Doan-Nguyen, M. R. Crump, D. C. Reifsnyder, C. B. Murray, and C. R. Kagan, J. Am. Chem. Soc. 133, 15753 (2011).
- ²⁷G. Li, J. Huang, Y. Li, J. Tang, and Y. Jiang, Nano Res. **12**, 109 (2019).
- ²⁸C. R. Kagan, E. Lifshitz, E. H. Sargent, and D. V. Talapin, Science **353**, 6302 (2016).
- ²⁹C.-H. M. Chuang, P. R. Brown, V. Bulović, and M. G. Bawendi, Nat. Mater. 13, 796 (2014).
- ³⁰ J. Xu, O. Voznyy, M. Liu, A. R. Kirmani, G. Walters, R. Munir, M. Abdelsamie, A. H. Proppe, A. Sarkar, F. P. García de Arquer, M. Wei, B. Sun, M. Liu, O. Ouellette, R. Quintero-Bermudez, J. Li, J. Fan, L. Quan, P. Todorovic, H. Tan, S. Hoogland, S. O. Kelley, M. Stefik, A. Amassian, and E. H. Sargent, Nat. Nanotechnol. 13, 456 (2018).
- D. M. Kroupa, M. Vörös, N. P. Brawand, B. W. McNichols, E. M. Miller, J. Gu,
 A. J. Nozik, A. Sellinger, G. Galli, and M. C. Beard, Nat. Commun. 8, 15257 (2017).
 P. R. Brown, D. Kim, R. R. Lunt, N. Zhao, M. G. Bawendi, J. C. Grossman, and
 V. Bulović, ACS Nano 8, 5863 (2014).
- ³³ Q. Shang, B. D. Piercy, M. D. Losego, and T. Lian, J. Phys. Chem. C **123**, 21415 (2019).
- ³⁴P. Guyot-Sionnest, B. Wehrenberg, and D. Yu, J. Chem. Phys. **123**, 074709 (2005)
- ³⁵H. McDaniel, P. E. Heil, C.-L. Tsai, K. Kim, and M. Shim, ACS Nano 5, 7677 (2011).
- 36 J. C. Flanagan and M. Shim, J. Phys. Chem. C 119, 20162 (2015).
- ³⁷J. Tang, H. Liu, D. Zhitomirsky, S. Hoogland, X. Wang, M. Furukawa, L. Levina, and E. H. Sargent, Nano Lett. 12, 4889 (2012).
- ³⁸ A. H. Ip, S. M. Thon, S. Hoogland, O. Voznyy, D. Zhitomirsky, R. Debnath, L. Levina, L. R. Rollny, G. H. Carey, and A. Fischer, Nat. Nanotechnol. 7, 577 (2012).
- ³⁹Z. Ning, O. Voznyy, J. Pan, S. Hoogland, V. Adinolfi, J. Xu, M. Li, A. R. Kirmani, J.-P. Sun, and J. Minor, Nat. Mater. 13, 822 (2014).
- ⁴⁰J. Song, O. Wang, H. Shen, Q. Lin, Z. Li, L. Wang, X. Zhang, and L. S. Li, Adv. Funct. Mater. 29, 1808377 (2019).
- ⁴¹ J.-Y. Yoo, W. H. Jung, C. W. Lee, B. D. Chin, J.-G. Kim, and J. S. Kim, Org. Electron. 99, 106326 (2021).
- ⁴²L. Wang, Y. Lv, J. Lin, J. Zhao, X. Liu, R. Zeng, X. Wang, and B. Zou, J. Mater. Chem. C 9, 2483 (2021).
- ⁴³ H. Zhang, Q. Su, and S. Chen, Adv. Opt. Mater. **8**, 1902092 (2020).

- ⁴⁴K.-H. Lee, J.-H. Lee, H.-D. Kang, B. Park, Y. Kwon, H. Ko, C. Lee, J. Lee, and H. Yang, ACS Nano 8, 4893 (2014).
- ⁴⁵ D. Kim, Y. Fu, J. Kim, K.-h. Lee, H. Kim, H. Yang, and H. Chae, Nanotechnology 27, 245203 (2016).
- 46 H. Moon and H. Chae, Adv. Opt. Mater. 8, 1901314 (2020).
- ⁴⁷H. Shen, W. Cao, N. T. Shewmon, C. Yang, L. S. Li, and J. Xue, Nano Lett. 15, 1211 (2015).
- ⁴⁸ L. Chen, M.-H. Lee, Y. Wang, Y. S. Lau, A. A. Syed, and F. Zhu, J. Mater. Chem. C 6, 2596 (2018).
- ⁴⁹J. Chen, D. Song, Z. Xu, S. Zhao, B. Qiao, W. Zheng, P. Wang, X. Zheng, and W. Wu, Org. Electron. 75, 105412 (2019).
- $^{50}\mbox{S}$ F. Wuister, C. de Mello Donegá, and A. Meijerink, J. Phys. Chem. B 108, 17393 (2004).
- ⁵¹ C. Pu, X. Dai, Y. Shu, M. Zhu, Y. Deng, Y. Jin, and X. Peng, Nat. Commun. 11, 937 (2020).
- ⁵²C. Blauth, P. Mulvaney, and T. Hirai, J. Appl. Phys. **126**, 075501 (2019).
- ⁵³ W. Lee, J. Yeop, J. Heo, Y. J. Yoon, S. Y. Park, J. Jeong, Y. S. Shin, J. W. Kim, N. G. An, D. S. Kim, J. Park, and J. Y. Kim, Sci. Rep. 10, 18055 (2020).
- ⁵⁴M. Jones, J. Nedeljkovic, R. J. Ellingson, A. J. Nozik, and G. Rumbles, J. Phys. Chem. B **107**, 11346 (2003).
- ⁵⁵T. Zhao, E. D. Goodwin, J. Guo, H. Wang, B. T. Diroll, C. B. Murray, and C. R. Kagan, ACS Nano 10, 9267 (2016).